

INDUCTIVELY COUPLED PLASMA ETCHING ON GaN

By

SITI AZLINA BINTI ROSLI

**Thesis submitted in fulfillment of the requirements for the degree of
Master of Science**

January 2010

ACKNOWLEDGEMENTS

Firstly, I would like to express my deepest gratitude to my supervisor, Associate Prof. Dr Azlan Abdul Aziz, for his guidance and support throughout the course of my research. He has been more than helpful in creating opportunities for priceless learning experience during his supervision. I also admire his patience with my pace of work. I also would like to sincerely thank Associate Prof. Dr. Roslan, for additional advice and help. Without his patience, guidance and constant supports, this work would not have been possible.

Secondly, my sincere thanks go to Mrs. Ee Bee Choo, Mr. Jamil, Mr. Hazhar and Mr. Mokhtar for their generous help and technical support offered during my laboratorial work. Their patience when working with me during my experiments is truly appreciated as my work can be very repetitive and unexciting from others point of view. I would also like to thank my research colleagues, especially Dr Maghdy, Ms Mazlindawati and my entire colleague especially at N.O.R lab for their assistance in research, ingenious ideas during discussion and lasting friendship together.

Last but most importantly, I wish to acknowledge the care and encouragement given by my loving parents and my siblings. Thank you very much for supporting me in so many ways from the beginning until the end.

TABLE OF CONTENTS

	Page
ACKNOWLEDGEMENTS	ii
TABLE OF CONTENTS	iii
LIST OF TABLES	vii
LIST OF FIGURES	viii
LIST OF SYMBOLS	xii
LIST OF ABBREVIATION	xiv
ABSTRAK	xvi
ABSTRACT	xviii
CHAPTER 1 : INTRODUCTION	1
1.1 Introduction	1
1.2 III- V Nitrides for Device Applications	1
1.2.1 Gallium Nitrides	4
1.2.2 Lack of suitable etchants	5
1.2.3 Dry Etching	6
1.3 Research Objectives	8
1.4 Outline of the thesis	9
CHAPTER 2 : THEORY OF PLASMA ETCHING	10
2.1 Introduction	10
2.2 Etching	10
2.3 Wet Etching	11
2.3.1 General Principles of Wet Etching	11
2.4 Dry Etching	12
2.4.1 Dry Processing	12
2.4.2 Plasma Fundamentals	13
2.4.3 Paschen Law	15
2.4.4 The formation of a DC voltage	16

2.4.5	Influence of DC Bias	19
2.4.5.1	Influence of the dimensions of the reactor and etching mode	19
2.4.5.2	Influence of the plasma parameters	20
2.4.5.2.1	Gases and Flow	20
2.4.5.2.2	Pressure	21
2.4.5.2.3	Power	22
2.4.6	Sheath Formation	22
2.4.7	Potential Distribution	24
2.4.8	Mechanisms of Dry Etching	26
2.5	Dry Etching Technique	29
2.5.1	Plasma Etching (PE)	31
2.5.2	Reactive Ion Etching (RIE)	32
2.5.3	Inductively Coupled Plasma Etching (ICP)	34
2.5.3.1	Anisotropic	39
2.5.4	Literature review of chlorine based plasma etching on GaN.	41
2.5.4.1	Chlorine based- dry etching	42
CHAPTER 3 : INSTRUMENTATIONS		48
3.1	Introduction	48
3.2	Film Thickness Measurements	48
3.2.1	Filmetrics	48
3.3	Physical microscopy	49
3.3.1	Scanning Electron Microscopy (SEM)	49
3.3.2	Atomic Force Microscopy (AFM)	52
3.4	Plasmalab 80Plus ICP-RIE System	53
3.5	Physical metal deposition	55
3.5.1	Thermal evaporator	55

CHAPTER 4 : FABRICATION	58
4.1 Introduction	58
4.2 Wafer cleaning and native oxide removal	58
4.3 Mask design	59
4.3.1 Linear and square mask fabrication	59
4.3.2 Optical lithography	61
4.3.2.1 Procedures of the optical lithography process	61
4.3.3 Procedures of the Electron Beam Lithography	64
4.4 Metallization utilizing thermal evaporator	65
4.4.1 Film Thickness	66
4.5 Lift-off process	66
4.6 Summary of the fabrication flow	67
CHAPTER 5 : STUDY OF THE EFFECTS OF Cl₂/Ar On GaN ETCHING	70
5.1 Introduction	70
5.2 Effects of mixtures of Argon	70
5.3 AFM results	73
5.4 SEM results	76
5.5 Effects of pressure	78
5.6 Effects of ICP power	81
5.7 Pattern of cross section observation for GaN using Electron Beam Lithography	84
CHAPTER 6 : STUDY OF THE EFFECTS OF Cl₂/H₂ On GaN ETCHING	86
6.1 Introduction	86
6.2 Effects of mixtures of Hydrogen	86
6.3 AFM results	89
6.4 SEM results	91

6.5	Effects of pressure	94
6.6	Effects of ICP power	97
6.7	Comparison of additive gases of Ar and H ₂ into Cl ₂	99
CHAPTER 7 : CONCLUSIONS AND FUTURE WORKS		101
REFERENCE		104
PUBLICATION AND SEMINARS		110
APPENDICES		
Appendix A	The location of major component in 80Plus Plasmalab ICP-RIE machine	112
Appendix B	Physical Properties of Nickel (Ni)	114

LIST OF TABLE

Table 1.1	Comparison of 300 K semiconductor material properties. (Adapted from Sawin, 1985).	3
Table 2.1	The distinctions between the two rate limiting steps.	11
Table 2.2	Important reactions in plasma (David, 1999).	15
Table 2.3	Boiling points for possible etches products of III-V nitrides etched in halogen- or CH ₄ /H ₂ -based plasmas. (Adapted from Pearton, 2000)	41
Table 2.4	Summary of etch rate results for GaN with different plasma chemistries in ICP technique (Rosli et al. (2005).	47
Table 4.1	The properties of Gallium Nitrides (GaN)	57
Table 4.2	Thickness of Ni fabricated on GaN	65
Table 4.3	Flow of pattern transfer from the mask to the wafer	67
Table 4.4	Description of the order in fabrication process	68
Table 6.1	Gas for GaN and trench etching with their main plasma radicals and products.	86

LIST OF FIGURES

Fig 1.1	The various ternary and quaternary materials used for LEDs with the wavelength ranges indicated. (Adapted from Pearton <i>et al.</i> , 2000)	2
Fig 1.2	Bandgap of hexagonal (a-phase) and cubic (b-phase) InN, GaN, and AlN and their alloys versus lattice constant a_0 . (Adapted from Pearton <i>et al.</i> , 2000).	3
Fig 2.1	Physical and chemical processes in a plasma.	12
Fig 2.2	DC and AC voltage on the powered	18
Fig 2.3	DC voltage in the plasma reactor in RIE mode	18
Fig 2.4	Schematic of simplified plasma etch reactor.	24
Fig 2.5	Potential distribution in RF discharge.	25
Fig 2.6	The four mechanisms of plasma etching: (a) sputtering, (b) purely chemical, (c) ion-enhanced energetic mechanism, (d) ion-enhanced inhibitor.	28
Fig 2.7	Schematic chamber diagrams of representative etching techniques	30
Fig 2.8	A schematic of RIE	32
Fig 2.9	Schematic diagram of DC self-bias in RIE system.	34
Fig 2.10	Schematic of a typical ICP system and Dual-Frequency Plasma Reactor	35
Fig 2.11	Pressure versus time of etching	39
Fig 2.12	Illustrative figure to emphasize the fact that sidewalls on etched featured are not subject to extensive energetic particle bombardment (Sree Harsha, 2006).	40
Fig 3.1	Filmetrics F20 System	49
Fig 3.2	The schematic diagram of a scanning electron microscope.	51
Fig 3.3	Scanning electron microscope (SEM) for high magnification optical observation combined with energy dispersive spectroscopy (EDS) system	51
Fig 3.4	Atomic force microscope (AFM) utilized to characterize the surface morphology of the samples	53
Fig 3.5	a) Schematic of the Plasmalab 80Plus ICP tool b) Full System of Plasmalab 80Plus System ICP-RIE	54
Fig 3.6	Diagram of the thermal evaporator	57
Fig 3.7	Picture of the thermal evaporator in the lab	57
Fig 4.1	(a) linear mask used to fabricate and (b) square pattern used to fabricate.	60

Fig 4.2	(a) well developed sample using linear mask to fabricate, (b) failed attempt sample using linear mask in fabrication, (c) well developed sample using square mask to fabricate and (d) failed attempt sample using square mask in fabrication	63
Fig 4.3	Lift-off method utilized to fabricate linear and square structures	66
Fig 4.4	Illustrations of the schematics for the fabrication process	68
Fig 5.1	Effects of flow rates of argon (sccm) on etching rates ($\text{\AA}/\text{min}$) and DC bias (-V) for n-GaN with Cl_2/Ar chemistries. Initially, the etch rates increased with respect to the flow rates of Ar and then decreased abruptly after 20 sccm Ar.	72
Fig 5.2	Effects of flow rates of argon (sccm) on etching rates ($\text{\AA}/\text{min}$) and DC bias (-V) for p-GaN with Cl_2/Ar chemistries. It showed similar results as n-GaN.	73
Fig 5.3	AFM measurement results for n-GaN	74
Fig 5.4	AFM measurement results for p-GaN	75
Fig 5.5	Effects of RMS Roughness (nm) of surface on flow rates of argon (sccm) for n-GaN and p-GaN with Cl_2/Ar chemistries. The surface roughness remained relatively reduced as the Ar flow rate increased.	75
Fig 5.6	SEM pictures of the sidewalls in etched patterns for n-GaN using: a) 60Cl_2 sccm, b) $60\text{Cl}_2/20\text{Ar}$ sccm, c) $60\text{Cl}_2/40\text{Ar}$ sccm, and d) $60\text{Cl}_2/60\text{Ar}$ sccm.	76
Fig 5.7	SEM pictures of the sidewalls in etched patterns for p-GaN using a) $60\text{Cl}_2/20\text{Ar}$ sccm, b) $60\text{Cl}_2/40\text{Ar}$ sccm, and c) $60\text{Cl}_2/60\text{Ar}$ sccm.	77
Fig 5.8	Effects of pressure on etching rates and DC bias for n-GaN with Cl_2/Ar chemistries. The etching rates increased as the addition of chamber pressure and reach the maximum etching rate at 5mTorr.	78
Fig 5.9	Effects of pressure on etching rates and DC bias for p-GaN with Cl_2/Ar chemistries. Initially, the etching rates increased with respect to the addition of chamber pressure and then decreased abruptly after 5mTorr.	79
Fig 5.10	Effects of RMS Roughness (nm) of chamber pressure (mTorr) for n-GaN and p-GaN with Cl_2/Ar chemistries. The surface roughness remained relatively gained as the addition of chamber pressure.	80
Fig 5.11	Effects of ICP power on etching rates and DC bias for n-GaN with Cl_2/Ar chemistries. The etching rates increased as the addition of ICP power and reach the	81

maximum etching rate at 200W.

Fig 5.12	Effects of ICP power on etching rates and DC bias for p-GaN with Cl ₂ /Ar chemistries. The etching rates increased as the addition of ICP power and reach the maximum etching rate at 200W. This result was same as n-GaN.	82
Fig 5.13	Effects of RMS Roughness (nm) of ICP power (W) for n-GaN and p-GaN with Cl ₂ /Ar chemistries. The surface roughness remained relatively gained as the addition of ICP power.	83
Fig 5.14	SEM pictures of the sidewalls in etched patterns for n-GaN using 60Cl ₂ /20Ar sccm, a) and b) size of the pattern, and c) and d) smooth sidewalls and anisotropy.	85
Fig 6.1	Effects of n-GaN etch rates (Å/min) and DC bias (-V) as a function of flow rates of H ₂ (sccm). The etch rate gain steadily with increased flow rates of H ₂ and slightly decreased after 15 sccm H ₂ .	87
Fig 6.2	Effects of p-GaN etch rates (Å/min) and DC bias (-V) versus flow rates of H ₂ (sccm). The etch rate decreased abruptly after 15 sccm H ₂ .	88
Fig 6.3	AFM measurement results for n-GaN	89
Fig 6.4	AFM measurement results for p-GaN	90
Fig 6.5	Flow Rates of H ₂ (sccm) versus RMS roughness (nm). The rms roughness for n-GaN etched decreased as the flow rates of H ₂ increased and this result was similar to p-GaN.	90
Fig 6.6	SEM pictures of the sidewalls in etched patterns for n GaN using: a) 30Cl ₂ sccm, b) 30Cl ₂ /15H ₂ sccm, and c) 30Cl ₂ /30H ₂ sccm.	92
Fig 6.7	SEM pictures of the sidewalls in etched patterns for p-GaN using; a) 30Cl ₂ /10H ₂ sccm, b) 30Cl ₂ /15H ₂ sccm and c) 30Cl ₂ /30H ₂ sccm	93
Fig 6.8	Effects of chamber pressure (mTorr) versus etching rates (Å/min) for n-GaN. The etching rates for n-GaN decreased as the pressure increased.	94
Fig 6.9	Effects of chamber pressure (mTorr) versus etching rates (Å/min). The etching rates for p-GaN decreased as the pressure increased and this result was similar to n-GaN.	95
Fig 6.10	Effects of chamber pressure (mTorr) versus RMS roughness (nm). The rms roughness for n-GaN etched increased as the chamber pressure increased and this result was similar to p-GaN.	96

Fig 6.11	Effects of ICP power on etching rates and DC bias for n-GaN with Cl ₂ /H ₂ chemistries. The etching rates increased as the addition of ICP power and reach the maximum etching rate at 200W.	97
Fig 6.12	Effects of ICP power on etching rates and DC bias for p-GaN with Cl ₂ /H ₂ chemistries. The etching rates increased as the addition of ICP power and reach the maximum etching rate at 200W. This result was same as n-GaN.	98
Fig 6.13	Effects of ICP power (W) versus RMS roughness (nm). The rms roughness for n-GaN etched gained as the ICP power increased and this result was similar to p-GaN.	99
Fig 6.14	Effects of additives gases of Cl ₂ chemistries flow rates (Ar and H ₂) versus etch rates and roughness, respectively.	100

LIST OF SYMBOLS

A	Area (cm^2)
d	Distance (cm)
e	Electron
ξ	Electric field (V/cm)
E_F	Fermi energy (eV)
E_g	Band gap (eV)
E_V	Valence band edge (eV)
h	Planck's constant (6.626×10^{-34} J.s)
I	Current (A)
I_o	Saturation current (A)
I_{ph}	Photocurrent (A)
j	ion flux (mA/cm^2)
K_s	Semiconductor dielectric constant
k	Boltzmann's constant (8.617×10^{-5} eV/K)
L_D	Length of the CRT display
L_S	Length of the scanned sample
M	Magnification
m	Electron mass (9.11×10^{-31} kg)
N	Electron density (cm^{-2})
n	Diode ideality factor
n	Electron density (cm^{-3})
n	Index of refraction
N_h	Hole concentration (cm^{-3})
N_e	Electron concentration (cm^{-3})
N_{eff}	Effective carrier concentration (cm^{-3})
N_s	Interfacial state density
p	Hole density (cm^{-3})
q	Magnitude of electron charge (1.60×10^{-19} C)
Q	Charge (C)
Q	Charge density (C/cm^2)
Q_S	Semiconductor Charge density (C/cm^2)
R	Resistance (ohms)
R_H	Hall coefficient (cm^3/C)
R_{HS}	Sheet Hall coefficient (cm^2/C)
r_S	Series resistance (ohms)
s	Probe spacing (cm)
s	Distance from object
s'	Distance from image
T	Absolute temperature (K)
θ	Diffraction angle (degree)
V	Voltage (cm^3)
V_{bi}	Built-in potential (V)

v	Velocity (cm/s)
V_H	Hall voltage (V)
v_d	Drift velocity
v_e	Acceleration voltage
v_{th}	Average thermal velocity between collisions
V_p	Potential voltage
V_F	Floating potential
V_{DC}	Self-bias voltage
W	Molecular weight of the etched material (g/mol)
Y	Ratio of photocurrent to absorbed photon flux
χ	Semiconductor electron affinity (eV)
ϕ_e	Effective Schottky barrier height (V)
ϕ_b	Schottky barrier height (V)
ϕ_m	Metal work function (V)
ϕ_s	Semiconductor work function (V)
μ	Particle mobility
P	Pressure (Torr)
ρ	Resistivity (ohm.cm)
ρ_c	Specific contact resistivity (Ohms.cm ²)
r	Density of the material to be etched (g/cm ³)
R	Etch rates
s	Sputter yield
T	Absolute temperature
x_g	Gap width (angstrom, Å)
x	Effective depth penetration
$\Delta\phi$	Image-force lowering of barrier (V)
ϕ	Angle of incidence
λ	Mean free path
λ_e	De Broglie wavelength

LIST OF ABBREVIATIONS

AFM	Atomic force microscope
Ag	Argentum (Silver)
AlN	Aluminium Nitride
AlCl ₃	Aluminium tri chloride
A. Q	Aqua regia
Ar	Argon
ASTM	American Society for Testing Materials
A.U.	Arbitrary unit
Au	(Gold)
B. A	Boiling Aqua regia
BOE	Buffered Oxide etchant (HF: NH ₄ F: H ₂ O)
BHF	Buffered Hydrofluoric (NH ₄ F.HF)
CAD	Computer Aided Design
CBM	Conduction band minimum
CF ₄	Carbon Tetra fluoride / tetra fluorocarbon
CHF ₃	Carbon Hydro tri fluoride
Cl ₂	Chlorine
Cu	Copper
C-V	Capacitance-Voltage
CRT	Cathode Ray Display
DC	Direct current
DPI	Dot per Inch
EDX	Energy Dispersive X-ray
ELO	Epitaxial Lateral Overgrowth
FE	Field Emission
FET	Field Effect Transistor
Ga	Gallium
GaN	Gallium Nitride
GaAs	Gallium Arsenide
H ₂	Hydrogen
HBT	Heterojunction Bipolar Transistor
HCl	Hydrochloric
He	Helium
HEMT	High Electron Mobility Transistor
HF	Hydrofluoric
H ₂ SO ₄	Sulfuric Acid
IC	Integrated Circuit
ICP	Inductively Coupled Plasma
InP	Indium Phosphate
InGaAs	Indium Gallium Arsenide
InGaN	Indium Gallium Nitride
LD	Laser Diode
LED	Light Emitting Diode
M	Metal
MBE	Molecular Beam Epitaxial
MESFET	Metal-Semiconductor FET
MISFET	Metal-Insulator-Semiconductor FET

MOCVD	Metalorganic vapor deposition
MOSFET	Metal-Oxide-Semiconductor FET
MS	Metal Semiconductor
MOVPE	MetalOrganic vapor-phase epitaxial
MQW	Multi Quantum Well
Ni	Nickel
O ₂	Oxygen
O ₂ *	Excited state of O ₂
PC	Photocurrent
PE	Plasma Etching
PR	Photo resist
Pt	Platinum
RIE	Reactive Ion Etching
RF	Radio Frequency
rms	Root mean square
SBH	Schottky Barrier Height
SC	Semiconductor
sccm	Standard Cubic Centimeters per Minute
SEM	Scanning Electron Microscope
SF ₆	Sulfur Tetra fluorides
Si	Silicon
SLR	Single Lens Reflex
TFE	Thermionic Field Emission
UV	Ultra Violet
VBM	Valence-band maximum
XRD	X-ray Diffraction
Xe	Xenon

PUNARAN PLASMA YANG DIGANDINGKAN SECARA TERARUH TERHADAP GALLIUM NITRIDA

ABSTRAK

Dalam projek ini, penyelidikan difokuskan kepada kajian tentang pengaruh pelbagai campuran plasma (H_2 dan Ar) kepada Cl_2 sebagai gas asas pada GaN menggunakan punaran kering khususnya punaran plasma yang digandingkan secara teraruh (ICP) untuk mendapatkan anisotropik yang tinggi, struktur dinding yang tegak dan yang paling penting adalah untuk memperoleh kadar punaran yang tinggi. Pertama sekali, wafer itu difabrikasi menggunakan fotolitografi dan Nikel diselaputkan ke atas wafer n-GaN atau p-GaN melalui alat pengewapan untuk melakukan proses 'angkat-buang'. Selepas itu, wafer dipunarkan menggunakan alat ICP-RIE. Semasa proses itu, kadar aliran gas untuk Ar atau H_2 diubahkan manakala kadar Cl_2 ditetapkan pada 60sccm untuk setiap eksperimen. Keadaan yang diperlukan dalam eksperimen ini ialah 60sccm Cl_2 dan jumlah kadar aliran 60sccm Ar atau 30sccm H_2 . Manakala, kuasa ICP yang digunakan ialah 100W, 250W kuasa RIE dan 600W kuasa RF. Sebelum membuat punaran kepada sampel, satu set eksperimen yang ringkas dilakukan untuk memahami tentang perubahan dalam komposisi gas yang mempengaruhi kadar punaran. Untuk eksperimen ini, kadar aliran Ar diubah dari 0sccm hingga 60sccm atau 0sccm hingga 30sccm menggunakan gas H_2 , manakala kadar aliran Cl_2 ditetapkan pada 60sccm dan tekanan kebuk ditetapkan pada 1mTorr. Kemudian, pelbagai tekanan diubah bermula dari 1mTorr hingga 15mTorr untuk memerhatikan kesan kadar punaran dan bentuk permukaan sampel dan akhir sekali, kuasa ICP dikenakan dari 100W hingga 450W. Setelah selesai fabrikasi, pencirian morfologi permukaan ditentukan menggunakan Mikroskop Elektron yang Diimbas (SEM) dan Mikroskop Atom Dipaksa (AFM).

Mikroskop Elektron yang Diimbis (SEM) digunakan untuk mengukur kadar punaran, anisotropik, dan struktur dinding manakala Mikroskop Atom Dipaksa (AFM) pula digunakan untuk mencirikan morfologi permukaan sebagai Purata punca Kuasa Dua (rms) permukaan. Dari eksperimen yang dilakukan, penambahan 15sccm H₂ bersama dengan Cl₂ di dalam kebuk pada tekanan 5mTorr dan 200W kuasa ICP menyebabkan perolehan kadar punaran yang paling tinggi iaitu sebanyak 3000Å/min untuk n-GaN dan 1900 Å/min untuk p-GaN dan mempunyai permukaan yang licin dan anisotropik. Manakala untuk penambahan 20sccm Ar bersama dengan 60sccm Cl₂ pada tekanan 5mTorr dan 200W kuasa ICP, kadar punaran yang paling tinggi didapati melebihi kadar punaran H₂; 5000Å/min dan ~0.5nm dan permukaannya masih kekal licin; ~0.5nm for n-GaN and ~0.7nm for p-GaN. Oleh itu, penambahan H₂ kepada plasma klorin menyebabkan permukaan yang dipunar lebih licin dari Ar, manakala penambahan Ar pula menyebabkan kadar punaran yang paling tinggi dicapai dalam eksperimen ini.

INDUCTIVELY COUPLED PLASMA ETCHING ON GaN

ABSTRACT

In this project, the research mainly focused on the investigation of the influence of the various plasma mixtures (H_2 and Ar) in Cl_2 -based on GaN using dry etching majoring in Inductively Coupled Plasma etching to obtain highly anisotropic, vertical sidewalls structures and most importantly, highly etch rates for optimum device performance. First of all, the wafer was fabricated using the conventional photolithography method and the Ni metals were coated onto the n-GaN or p-GaN wafer through evaporator equipment to make lift-off process. After that, the wafer was etched using ICP-RIE machine. During the process, the gas flow rates for Ar or H_2 were varied while Cl_2 rates were held constant at 60sccm for all experiments. The conditions consisted of 60sccm of Cl_2 and the total flow rate 60sccm of Ar or 30sccm of H_2 . Meanwhile, ICP power, RIE power and RF power was held at 100W, 250W and 600W respectively. Prior to etching patterned samples, a simple set of experiments were conducted to get an understanding of how changes in gas composition affect the etch rate. For this experiment, the flow rate was varied from 0sccm to 60sccm using Ar gases or from 0sccm to 30sccm using H_2 gases, meanwhile the Cl_2 flow rates and the chamber pressure were held constant at 60sccm and 1mTorr, respectively. Then, the various pressures were varied starting of 1mTorr to 15mTorr to observe the effect of etch rates and the roughness of surface and lastly, the ICP power applied from 100W to 450W. After that, the wafer will be characterized using SEM and AFM. SEM will be used to measured the etch rates, anisotropic etch profiles and sidewalls meanwhile AFM has been used to quantify the etched surface morphology as root-mean-square (rms) roughness. From our

experiments, the addition of 15sccm H₂ together with Cl₂ in the chamber at 5mTor of pressure and 200W ICP power obtained high etching rate about 3000Å/min for n-GaN and 1900Å/min for p-GaN and smooth anisotropic pattern. Meanwhile, for addition of 60sccm Ar together with 20sccm Cl₂ at pressure of 5mTorr and 20W ICP power resulting the highest etch rates, better than the addition of H₂; 5000Å/min for n-GaN and 3300Å/min for p-GaN, while maintaining the smooth surface; ~0.5nm for n-GaN and ~0.7nm for p-GaN. Hence, it was found that the addition of H₂ to chlorine plasma distributed a smooth etched surface better than Ar, while addition of Ar resulting the highest etching rates for this research.

CHAPTER 1 INTRODUCTION

1.1 Introduction

This chapter was devoted to issues and theories that were relevant to the work in this research. This chapter begins with an elaboration about the fundamental properties of GaN, lack of suitable etchants and dry etching and ended the chapter with research objectives of this work.

1.2 III-V Nitrides for Device Applications

For the last three decades or so, the III-V semiconductor material system has been viewed as highly promising for semiconductor device applications at blue and ultraviolet (UV) wavelengths in much the same manner that its highly successful As-based and P-based counterparts have been exploited for infrared, red and yellow wavelength as shown in Figure 1.1. As members of the III-V nitrides family, AlN, GaN, InN and their alloys were all wide band gap materials, and can crystallize in both wurtzite and zincblende polytypes. Wurtzite GaN, AlN and InN have direct room temperature bandgaps of 3.4 eV, 6.2 eV and 1.9 eV, respectively (Figure 1.2). In cubic form, GaN and InN have direct bandgaps, while AlN was indirect. In view of the available wide range of direct bandgaps, GaN alloyed with AlN and InN may span a continuous range of direct bandgap energies throughout much of the visible spectrum well into the ultraviolet wavelengths. This makes the nitride system attractive for optoelectronic device applications, such as light emitting diodes (LEDs), laser diodes (LDs), and detectors, which were active in the green, blue or UV wavelengths (Strite, 1992).

Another area gaining a lot of attention for III-V nitrides was high temperature/high power electronics (Pearson, 2000). The interest stems from two

intrinsic properties of this group of semiconductors. The first was their wide bandgap nature. The wide bandgap materials such as GaN and SiC are promising for high temperature applications because they go intrinsic at much higher temperatures than materials like Ge, Si and GaAs. It means that GaN power devices can operate with less cooling and fewer high cost processing steps associated with complicated structures designed to maximize heat extraction. The second attractive property of III-V nitrides was that they have high breakdown fields. The critical electric field of the breakdown scales roughly with the square of the energy band gap, and was estimated to be >4 MV/cm for GaN (Ali, 1991), as compared to 0.2 and 0.4 MV/cm for Si and GaAs respectively. Other advantageous properties of III-V nitrides include high mechanical and thermal stability, large piezoelectric constants and the possibility of passivation by forming thin layers of Ga₂O₃ or Al₂O₃ with band gaps of 4.3 eV and 9.2 eV respectively.

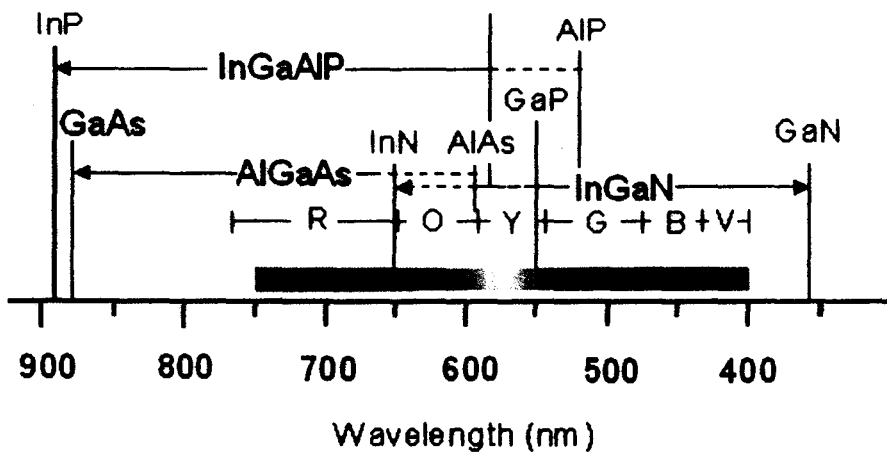


Fig. 1.1 The various ternary and quaternary materials used for LEDs with the wavelength ranges indicated (Adapted from Pearton *et al.*, 2000).

GaN has also excellent electron transport properties, including good mobility, and high saturated drift velocity (Sze, 1990). This makes it adequate for general electronics, and promising for microwave rectifiers, particularly. The material

properties associated with high temperature, high power, and high frequency application of GaN and several conventional semiconductors are summarized in Table 1.1. It was anticipated that GaN may eventually prove to be superior to SiC in this area.

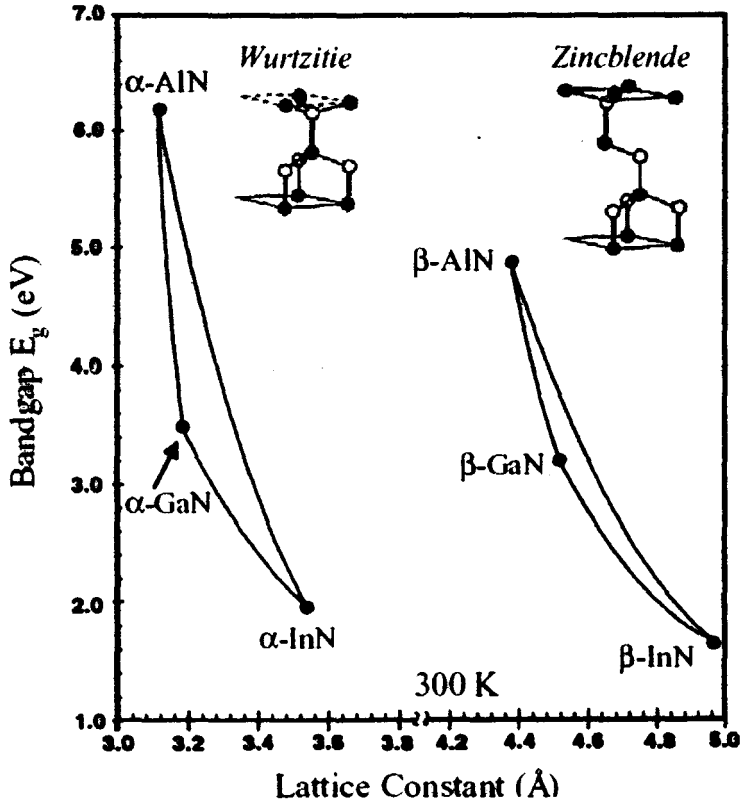


Fig. 1.2 Bandgap of hexagonal (a-phase) and cubic (b-phase) InN, GaN, and AlN and their alloys versus lattice constant a_0 (Adapted from Pearton *et al.*, 2000).

Table 1.1 Comparison of 300 K semiconductor material properties (Adapted from Sawin, 1985).

Property	Si	GaAs	4H-SiC	GaN
Bandgap E_g (eV)	1.12	1.42	3.25	3.40
Breakdown Field E_B (MV/cm)	0.25	0.4	3.0	4.0
Electron Mobility μ ($\text{cm}^2/\text{V}\cdot\text{s}$)	1350	6000	800	1300
Maximum Velocity v_s (10^7 cm/s)	1.0	2.0	2.0	3.0
Thermal Conductivity χ (W/cm \cdot K)	1.5	0.5	4.9	1.3
Dielectric Constant ϵ	11.8	12.8	9.7	9.0
CFOM = $\chi\epsilon\mu v_s E_B^2 / (\chi\epsilon\mu v_s E_B^2)_{\text{Si}}$	1	8	458	489

(CFOM= Combined Figure of Merit for high temperature/high power/high frequency applications).

1.2.1 Gallium Nitrides

Of all the III-V nitrides, gallium nitride or GaN was considerably the most intensely studied among the III-V nitride semiconductors. GaN was a direct and wide band gap semiconductor when compared to the more widely known Si as well as GaAs and SiC, to name among a few. With its superior radiation hardness and chemical stability, together with its large band gap characteristic, these properties have made GaN a suitable semiconductor material for device applications in the high-temperature and caustic environment as well as in space applications. GaN was also an attractive candidate for protective coatings due to its radiation hardness (Strite, 1992). Its wide band gap make it go intrinsic at a much higher temperature than materials like Ge, Si and GaAs, i.e. the intrinsic carrier concentration at any given temperature decreases exponentially with band gap, and therefore GaN and similar wide band gap materials are attractive for high temperature applications. Moreover, due to its many attractive features like higher sheet charge densities, higher mobilities, better charge confinement, and higher breakdown voltages, GaN was also a potential candidate for the application in electronic devices such as high temperature, high power and high frequency transistors (Ali, 1991, Sze, 1990, Pearton, 1999).

Unlike SiC, another widely studied large band gap semiconductor with demonstrated n- and p- type doping and excellent power device performance, one advantage of GaN as well as III-V nitrides was that they form direct band gap heterostructures, have better ohmic contacts and heterostructures., which eventually made III-V nitrides or GaN a more promising candidate than SiC in terms of application devices in optoelectronics (Razeghi, 1996).

The transparency of high quality GaN at wavelengths longer than the band gap make it an ideal material for fabricating photodetectors capable of rejecting near infrared and visible regions of the solar spectrum while retaining near unity quantum efficiency in the UV. Besides, in optoelectronics, GaN was primarily of interest for its potential as a blue and UV light emitter (Strite, 1992). GaN was most commonly observed as the wurtzite 2H polytype but it can also crystallize into a metastable zinc-blende 3C structure (Mizuta, 1986, Davis, 1989, Petrov, 1992, Strite, 1993). However, another structure, which was the rocksalt, or NaCl structure can also be induced in the GaN under very high pressures (Morkoc, 1999).

In general, GaN normally crystallizes in the wurtzite crystal structure, where it was grown on hexagonal substrates. On the other hand, the zinc blende structure can be grown on cubic substrates.

1.2.2 Lack of suitable etchant

The chemical stability of GaN provides a technological challenge, for example like when it comes to lithography (Maruska, 1996) where there have been many reports describing the resistance of GaN films to the conventional wet etching techniques used in semiconductor processing. There was no reliable wet chemical etchant that has been found for GaN. Maruska and Tietjen (1996) reported that GaN was insoluble in H₂O, acids, or bases at room temperature; however GaN did dissolve in hot alkali solutions, but at a very slow rate. Due to the difficulties of developing an established chemical etching process for GaN despite the efforts of many researchers, the attentions has shifted to dry etching; reactive ion etching (RIE) and high density plasma etching as the dominant patterning technique for III-V materials including GaN.

1.2.3 Dry etching

In general, many have reported excellent etch anisotropies suggesting that RIE was a highly suitable technology for GaN-based device processing. Reactive ion etching (RIE) was one of the dry etching techniques in common usage, which utilizes both the chemical and physical components of an etch mechanism. RIE plasmas are typically generated by applying radio frequency (rf) power of 13.56 MHz between two parallel electrodes in a reactive gas. Etching was typically performed at low pressures, ranging from a few mTorr up to 200 mTorr, which promotes anisotropic etching due to increased mean free paths and reduced collisional scattering of ions during acceleration in the sheath. RIE was by far the most popular dry etching technique used for conventional III-V materials, and takes advantage of the fact that there was a synergism between the physical and chemical etching mechanisms.

The use of high-density plasma etch systems, such as inductively coupled plasma (ICP) (Pearson, 2000) and electron cyclotron resonance (ECR), has resulted in improved etch characteristics for the III-V nitrides as compared to RIE. This observation was attributed to plasma densities which were 2-4 orders of magnitude higher than RIE thus improving the III-N bond breaking efficiency and the sputter desorption of etch products from the surface. Additionally, since ion energy and ion density can be more effectively decoupled, plasma induced damage was more readily controlled.

High density ICP plasmas were formed in a dielectric vessel encircled by an inductive coil into which rf power was applied. The alternating electric field between the coils induces a strong alternating magnetic field trapping electrons in the centre of the chamber and generating plasmas with uniform density and energy distribution.

By keeping ion and electron energy low, we can obtain low damage etching while maintaining fast etch rates.

Anisotropy was achieved by superimposing a rf bias on the sample. Generally, etch characteristics were dependent upon plasma parameters including ion energy (controlled by rf chuck power), plasma density (controlled by ICP source power), and operation pressure (the change in collisional frequency can result in changes in both ion energy and plasma density). ICP etching was generally believed to have several advantages including easier scale-up for production, improved plasma uniformity and lower cost of operation.

Good results for the III-V nitrides have been obtained in chlorine-based plasma under high ion energy conditions where the III-N bond breaking and the sputter desorption of etch products were most efficient. Unfortunately, the high energy plasma may induce significant damage and degrade both electrical and optical device performances. Lowering the ion energy and increasing the chemical activity in the plasma often results in much slower etch rates and less anisotropic profiles. It was necessary to pursue alternative etch platforms which combine high quality etch characteristics with low damage for III-V nitrides.

Additive gases have been introduced in order to obtain a vertical sidewall, since etching with pure Cl_2 generally leads to severe undercuts (Rommel, 2002). Cho et al. reported binary gas chemistries such as Cl_2/Ar , Cl_2/N_2 , Cl_2/H_2 and concluded that ICP discharges were well-suited to achieving smooth etched surfaces when appropriate plasma condition were used. Previous study has demonstrated that unintentionally doped successfully etched by ICP using Cl_2/Ar as the etching gases (Sheu, 1999). It has been shown that one can achieve a highly anisotropic etch with a high etching rate and smooth surface morphology by using Cl_2/Ar as the etching

gases. During such ICP etching, Cl_2 was used to provide reactive Cl radicals, chemically react with GaN to form volatile etch products, and then desorbed from the sample surface. On the other hand, Ar was used to perform physical etching so as to achieve an anisotropic etching. Cl_2/H_2 mixture has also been studied since the inclusion of H_2 in the plasma was found to increase etch rates and also improve surface morphology.

To date, only a few reports on the effect of gas additives to Cl_2 plasmas have been reported. Therefore, the effects of gas additives such as H_2 and Ar on the etch characteristics of an inductively coupled Cl_2 -based plasma have been chosen as a collection of recipes for this research. Each gas additive had unique effects on the etch rate, etch anisotropy, surface roughness and sidewall morphology, all of which require reliable control for device fabrication.

1.3 Research Objective

As the circuit complexity increases and device dimensions decrease, it was very necessary to choose right technique in order to get a highly anisotropic result. In this project, the research mainly focused on the investigation of the dry etching majoring in Inductively Coupled Plasma etching on GaN. To achieve the main objectives, several sub objectives have been identified:

1. To obtain recipes using gas combination (Ar and H_2) in Cl_2 -based on GaN.
2. To study the effects of Cl_2/Ar mixture on n-GaN and p-GaN etching.
3. To investigate the effects of Cl_2/H_2 mixture on n-GaN and p-GaN etching.

4. To get the formation of highly anisotropic and sidewalls structures.
5. To determine the smooth surfaces after etching to avoid stress concentration for selected recipes.

1.4 Outline of the thesis

The content of this thesis was organized as follows:-

The next chapter, Chapter 2, will cover GaN-related matters and theory that were relevant to the work in this research.

Chapter 3 was devoted to the instrumentation employed in this work. An explanation on the procedures and methods used, and also some principles underlying the operation of the instruments were covered.

Chapter 4 will discuss include the main topic/theory which was associated in the fabrication process as well as the discussions of methods used in obtaining the results for this research project.

In Chapter 5 and 6, the results of the effects of Cl_2/Ar and Cl_2/H_2 mixture on n-GaN and p-GaN etching from this research were presented, analysed and discussed.

The final chapter, Chapter 7 concludes the thesis with a summary of the research work. Conclusion of the results obtained and a few suggestions for future research were included.

CHAPTER 2 THEORY OF PLASMA ETCHING

2.1 Introduction

This chapter is devoted to the theories that are relevant to the work in this research such as general principles of etching; wet and dry etching, the process of etching and the fundamentals of plasmas. Meanwhile, the types and the technique of dry etching including the literature review of Cl₂-based plasma etching are explained at last topics in this chapter.

2.2 Etching

“*Etching*” is used to describe any technique by which material can be uniform removed from a wafer, or locally removed as in the transfer of patterns during fabrication of a microcircuit. Etching processes are divided into two major groups; wet etching (e.g. liquid chemicals) and dry etching (e.g. reactive gas plasmas). The basic mechanism of wet chemical etches of semiconductors is the formation of an oxide, or oxides on the surface, and the subsequent dissolution of the oxidized products by either acids or bases (Manos, 1989). The main advantage of this etching method is its simplicity, high selectivity, high throughput and low cost. However, these advantages do not apply to nitrides based material. GaN for example, electrolysis etches slowly at room temperature in hot alkalis and complex electrolytically using NaOH. Because of all this difficulties in obtaining reliable wet etching process, much work on nitride based etching are concentrated on dry etching processes. As such, we will only discuss briefly on wet etching and elaborate on the progress of dry etching throughout this chapter.

2.3 Wet Etching

2.3.1 General Principles of Wet Etching

Wet chemical etching of any material can be thought of as a sequence of five steps (Gandhi, 1983):

- 1) Transport of the reactant to the surface
- 2) Adsorption of the reactant
- 3) Reaction at the surface
- 4) Desorption of reaction products
- 5) Removal of reaction products away from the surface

Each of these three steps can function as a rate limiter and dominate the entire process. If the etch rate is controlled by the rate at which the reactant species can reach the surface, or the rate at which the reaction products are removed, the process is said to be diffusion-limited. If the etch rate is only limited by the rate of chemical reactions at the surface then the process is said to be reaction-rate limited (William, 1990). Some distinctions between the two rate limiting steps are as follows:

Table 2.1 The distinctions between the two rate limiting steps.

The attributes of <u>diffusion controlled reactions</u>	The attributes of <u>reaction-rate controlled reactions</u>
The activation energy is viscosity controlled, 1-6 kcal/mol and increases with stirring	The activation energy is typically 8-20 kcal/mol
All substances and crystal orientations etch at the same rate	The rate changes with etchant concentration
The reaction rate increases with agitation	The rate is not sensitive to agitation
The etch depth is proportional to the square root of etch time	The etch depth is linearly dependent on etch time

As with all chemical reactions, etching is sensitive to temperature. A 10°C increase in temperature can increase the etch rate by as much as a factor of two. Another consideration is the aging of etchant solutions. Some solutions may change

composition over time, depending on temperature and storage. All of these factors must be considered in establishing reproducible and controllable etching processes (William, 1990).

2.4 Dry Etching

2.4.1 Dry Processing

A useful model of both dry process equipment and the processing itself is the idea that dry process results come from a balance between physical and chemical processes at the wafer surface. Figure 2.1 illustrates how a process dominated by sputter etching at low pressure and high ion energy can be compared to a process dominated by chemical etching at high pressure and low ion energy. Typically, sputter etching processes provide anisotropic profiles but do not provide selective etching between the different films on the wafer such as the photo resist, the etch film and the layer under the etch film. Faceting of the mask is also characteristics of sputter etch processes. At the other extreme is purely chemical etching, which usually provides excellent selectivity between films that have different chemical composition but tend to etch with isotropic profiles. Successful etch processing occurs when the correct balance between these two extremes is struck.

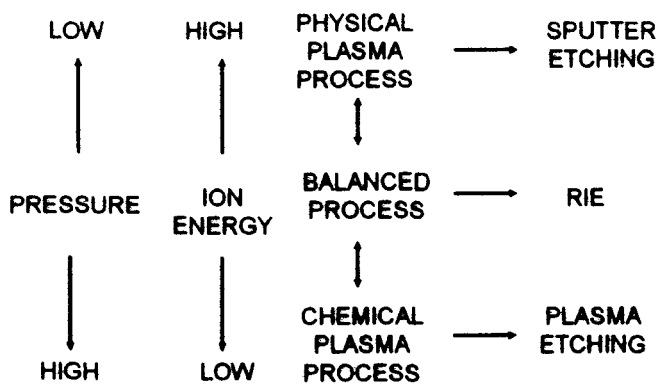


Fig. 2.1 Physical and chemical processes in a plasma

2.4.2 Plasma Fundamentals

Plasma is a gas which contains equal numbers of positive and negative charges; neutral atoms, radicals, or molecules; in addition to photons emitted from excited species. Radicals are molecule fragments with unsaturated bonds. Positive charge carriers are mostly singly ionized atoms, radicals, or molecules created by impact with energetic electrons. The majority of negative charges are free electrons. In the presence of atoms with high electron affinity, negatively charged ions can be created when these capture plasma electrons. Neutral atoms, radicals, and molecules can be at ground or excited state. Photons are emitted when excited species lose energy via spontaneous transitions to lower energy states. This latter process is the basis for the “glow” of the discharge.

Plasma can be created by applying an electric field of sufficient magnitude to a gas. The process can be initiated by an incident electron which gains kinetic energy from the applied electric field. The probability for the electron to collide with and transfer energy to a gas atom or molecule depends upon the electron energy, the gas pressure, and the dimensions of the plasma chamber. When a collision occurs, it results in ionization, excitation, or fragmentation of gas molecules. An ionizing collision generates an electron-ion pair. The two new charged particles are accelerated in the electric field and can in turn collide with and ionize other gas particles. As this process continues, the gas breaks down and plasma is created. The charged particles can be neutralized by recombination within the plasma or at the chamber walls. For plasma to be sustained, however, the rate of ionization of gas atoms or molecules must be equal to the rate of electron and ion recombination.

Collisions can result in fragmentation of gas molecules into atoms or molecules of smaller size or, for smaller electron energies, in excitation of atoms or

molecules to higher energy levels. Some important chemical and physical processes that occur in plasma are summarized in Table 2.2 (Sawin, 1985). At thermal equilibrium the particles can be assumed to move randomly at an average thermal velocity between collisions, approximated by

$$v_{th} \cong \sqrt{\frac{3kT}{m}} \quad (2.1)$$

where k is Boltzmann's constant ($k = 8.62 \times 10^{-5}$ eV/K), T the absolute temperature, and m the particle mass. Because of their very small mass, electrons travel at much higher thermal velocity than gas atoms or molecules. The motion of charged particles under the influence of an electric field is described in terms of a drift velocity, v_d , given by

$$v_d = \mu E, \quad (2.2)$$

where μ is the particle mobility, and E the electric field.

Electrons also drift at a much higher velocity than ions. As electrons gain kinetic energy from the electric field, their effective temperatures increase above the gas temperature. While the temperature of the atoms and molecules in the gas remains near ambient, electrons can attain high average energies, typically 1-10 eV, corresponding to an effective electron temperature of 10^4 - 10^5 K (Fonash, 1985).

This energy is transferred to the gas by collision processes in which ions and highly reactive species are created. It is this property of the plasma that allows high-temperature type reactions to occur at low ambient temperatures and permits the use of temperature sensitive materials such as organic resist masks for etching. The average distance travelled by particles between collisions, called the mean free path λ , depends on the species and gas pressure following the relation

$$\lambda = \frac{5 \times 10^{-3}}{P} (cm) \quad (2.3)$$

where P is the pressure in Torr. The electron density in plasmas of interest ranges from $10^9 - 10^{12} \text{ cm}^{-3}$. It follows that the degree of ionization is very small; in typical reactors used for etching only 10^{-4} to 10^{-7} of the gas molecules are ionized (El Kareh, 1995).

Table 2.2 Important reactions in plasma (David, 1999).

Reaction	Example
Positive ionization	$\text{Ar} + e \rightarrow \text{Ar}^+ + 2e$ $\text{O}_2 + e \rightarrow \text{O}_2^+ + 2e$
Dissociative	$\text{CF}_4 + e \rightarrow \text{CF}_3 + \text{F} + 2e$
Fragmentation	$\text{CF}_3\text{Cl} + e \rightarrow \text{CF}_3 + \text{Cl}e^-$ $\text{C}_2\text{F}_6 + e \rightarrow 2\text{CF}_3 + e$
Dissociative attachment	$\text{CF}_4 + e \rightarrow \text{CF}_3 + \text{F}^-$
Dissociative ionization with attachment	$\text{CF}_4 + e \rightarrow \text{CF}_3 + \text{F}^- + e$
Excitation	$\text{O}_2 + e \rightarrow \text{O}_2^* + e^-$
Photoemission	$\text{O}_2^* \rightarrow \text{O}_2 + h\nu$

O_2^* is the excited state of O_2

2.4.3 Paschen Law (Ledernez, 2009)

The first Townsend coefficient α is the probability to ionize a gas neutral by collision per unit length of path, i.e. it is the number of collision per unit length of path times the ionization probability per collision. Hence:

$$\alpha = \frac{1}{\lambda_e} \times \exp\left(-\frac{E_i}{E_e}\right) \quad (2.4)$$

with λ_e the electron mean free path, E_i the ionization energy of the gas, E_e the electron energy colliding with the gas neutral. Equation (2.4) is more commonly known as (Cobine, 1958): $\alpha = A p \exp\left(-\frac{B p}{E}\right)$ with $E_e = e \lambda_e E$. Assuming that the electric field is uniform before the gas breakdown ($E = V_b / d$), Eq. (2.4) can be transformed to:

$$V_{br} = \frac{B p d}{C + \ln(p d)} \quad (2.5)$$

With $\lambda_e = \frac{k_B T}{\sigma_{ei} p}$, one can deduce:

$$A = \frac{\sigma_{ei}}{kT} \quad (2.6)$$

and the Paschen coefficients:

$$B = \frac{\sigma_{ei} E_i}{ekT} \quad (2.7)$$

$$C = \ln\left(\frac{\sigma_{ei}}{\alpha dkT}\right) \quad (2.8)$$

where σ_{ei} is the electron impact ionization cross section (in m^2), E_i is the ionization energy of the gas (in J), e the elementary charge (in C), k the Boltzmann constant, T the temperature (in K).

2.4.4 The formation of a DC voltage. (Verdonck, 1990)

Plasma is a (partially) ionized gas. In the plasmas we deal with, free electrons collide with neutral atoms/molecules and, through a dissociative process, they can remove one electron from the atom/molecule, which gives a net result of 2 electrons and 1 ion. Depending on the energy of the incoming electron, this collision can result also in other species, such as negative ions, because of electron association, excited molecules, neutral atoms and ions. The light emitted by the plasma is due to the return of excited electrons to their ground state. As the energies between the electrons states are well defined for each element, each gas will emit light at specific wavelengths, which will give us the possibility to analyse the plasma.

The power is applied to the lower or the upper electrode (or in some special cases to the reactor walls). In general the frequency of the applied power is 13.56 MHz. A so-called dark sheath is formed in the neighbourhood of all surfaces in the reactor, electrodes and walls. This dark sheath can be considered as some kind of

dielectric or a capacitor. So, the applied power is transmitted to the plasma through a capacitor.

At frequencies between 1 MHz and 100 MHz, the free electrons are able to follow the variations of the applied electric field and, unless they suffer a collision, they can gain considerable energy, of the order of some hundred eV. On the other hand, in this frequency range, the movement of the much heavier (positive) ions is very little influenced (one may simplify that they are not influenced) by these electric fields: their energy comes completely from the thermal energy of the environment and is of the order of a few hundredths of an eV (i.e., $\sim 0.01\text{eV}$).

In the pressure range of these plasmas, from a few mTorr to a few hundreds of mTorr, the electrons will travel much longer distances than the ions, and in this way, they will much more frequently collide with the reactor walls and electrodes and consequently be removed from the plasma. This would leave the plasma positively charged. However, plasmas remain neutral. To guarantee this neutrality, a DC electric field has to be formed in such a way that the electrons are repelled from the walls. The capacitor between the power generator and the electrode helps to form the DC charge. During the first few cycles, electrons generated in the plasma escape to the electrode and charge the capacitor negatively. In this way, a negative DC bias voltage is formed on the electrode, which repels the electrons. The AC voltage becomes then superposed on this negative DC voltage as shown in Figure 2.2.

Free electrons escape from the plasma in higher numbers to the walls than ions do. So, one also needs a certain DC voltage to repel the electrons from the walls. In this way, one can understand that the DC voltage of the plasma will always be the most positive of all the DC voltages in the reactor. Figure 2.3 shows how the DC voltage varies between the lower and upper electrode. This figure indicates clearly

how the electrons are repelled from the walls and electrode towards the plasma. The ions are attracted towards the wall. However, because of their large mass, only the ions which arrive “by coincidence” at the interface of the plasma with the dark sheath will be attracted towards the electrodes or the walls. Within the plasma, the ions are not influenced by the electric fields and move randomly.

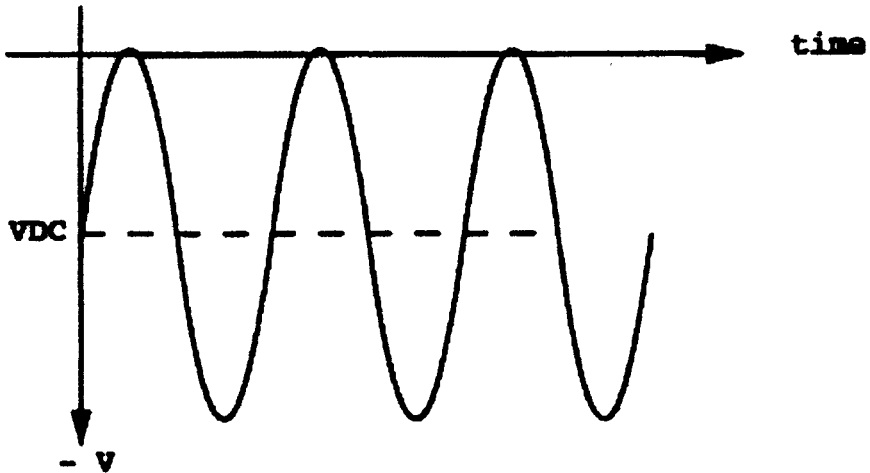


Fig. 2.2 DC and AC voltage on the powered (Adapted from Verdonck, 1990)

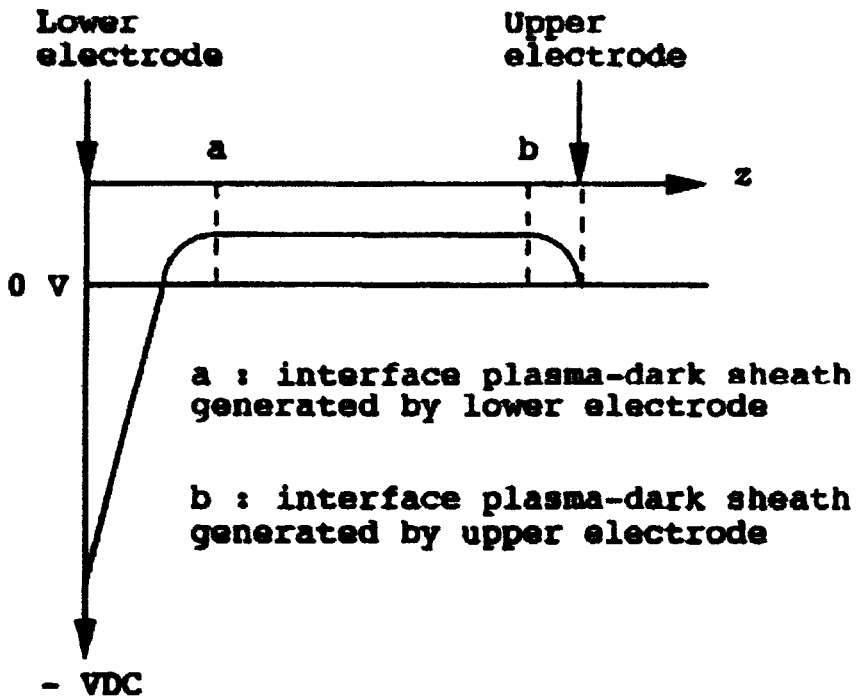


Fig. 2.3 DC voltage in the plasma reactor in RIE mode (Adapted from Verdonck, 1990)

In most reactors, one can clearly observe this so-called dark sheath as a region with less luminosity than the bulk of the plasma. In this region, the density and energy of the free electrons is lower. Therefore, less collisions with molecules will occur, causing less excitations of electrons (bound to molecules) and therefore less photons will be emitted from this region.

2.4.5 Influence of DC Bias (Verdonck, 1990)

The value of the DC voltage is influenced by many parameters. It depends in the first place on the dimensions of the etching reactor. It also depends on the plasma process (gas, flow, pressure, power etc).

2.4.5.1 Influence of the dimensions of the reactor and etching mode

One can demonstrate that:

$$|V_{DC}| \sim (A_1/A_2)^n \quad (2.9)$$

with the V_{DC} the voltage drop between plasma and electrode 2, A_1 the area of electrode 1, A_2 the area of electrode 2, n an exponential factor, which is typically between 1 and 2. Formula 2.9 is valid for whatever electrode is powered. If electrode 1 is powered and electrode 2 is grounded, V_{DC} is in the case the DC potential of the plasma.

One can prove that $n = 1$ or that $n = 2$, depending on the (very reasonable) assumptions one makes about the plasma. Anyway, the modulus of the DC voltage will increase with the ratio of grounded surface area. In RIE systems, the powered electrode has in general much less area than the grounded surfaces, resulting in a large negative DC voltage on the lower electrode. The consequences on the etching

results will be discussed later. In PE systems, the upper electrode is powered and the lower electrode is in general grounded, together with the walls. This results in general in a small voltage drop between plasma and lower electrode. One can decrease the voltage drop between plasma and electrode even more, when one leaves the electrode floating i.e. no electrical connection is made to the lower electrode.

2.4.5.2 Influence of the plasma parameters

In general, the dimensions of the reactor are fixed. In this case, one can influence the DC voltage by the process parameters. One should remember that the DC voltage is created to repel electrons. Therefore, the higher the electron density and the higher the electron energy, the higher the modulus of the DC voltage will be: a more negative voltage is necessary to repel a larger number of electrons, with higher energies. Using this reasoning, one is able to predict the tendencies of the DC bias voltage.

2.4.5.2.1 Gases and Flow

The electronegativity of used gases is a determining factor. When all other process parameters remain constant, the electronegativity of the gas will determine the DC voltage. Gases with low electronegativity, such as O₂, N₂ etc. have very negative DC bias voltages. Fluorine, chlorine and bromine containing gases are much more electronegative: the atoms of group VII are very prone to absorb any free electron which passes nearby. In this way, these gases decrease the density of the free electrons in the plasma (increasing the number of negative ions). Fluorine containing gases are more electronegative than chlorine containing gases, which are more electronegative than bromine containing gases. SF₆ is a very electronegative

gas: its main use is in fact as an insulator gas in places with high electric fields, e.g. around linear accelerators. When all other plasma parameters remain the same, the DC voltage of SF₆ plasma can be a factor of 10 less than the DC voltage of N₂ plasma. The absolute flow of the gases does in general not affect the DC voltage. If a mixture of gases is used, the DC bias will be a monotonically increasing function of the relative flows of the gases. In general, the DC bias tends to become rapidly more negative when a small flow of a gas with low electronegativity is entered in the plasma. Small flows of electronegative gases do not influence the DC bias very much.

2.4.5.2.2 Pressure

The pressure of the plasma does also influence the DC bias voltage, but to explain its influence is a little more complicated. At higher pressure, more molecules are available for the electrons to collide with and to generate a new free electron - and a positive ion. In this way, an increase in pressure would increase the number of free electrons, turning the DC voltage more negative. On the other hand, an increase in pressure increases the density of species, i.e. it decreases the mean free path of the electrons before colliding. In this way, the electrons will gain less energy before colliding. This decrease in energy results in less formation of a new electron-positive ion pair. This mechanism decreases the formation of free electrons and ions. So, one has two tendencies in opposite ways. In the pressure ranges used for plasma etching, one can observe that in the 1- (approximately) 100 mTorr range, the number of free electrons increases, the plasma becomes more dense with increasing pressure. At higher pressure, the plasma density decrease with pressure. The DC voltage is also a function of the energy of the free electrons. At higher pressure, electrons suffer more

collisions, therefore they gain less energy between collisions. The electron energy decreases with pressure. Taking all these mechanisms in account, one can understand that the DC bias voltage becomes less negative with increasing pressure.

2.4.5.2.3 Power

The influence of power is straightforward: an increase of power increases both the density and the energy of the free electrons. Therefore, the DC voltage becomes more negative with increasing power.

2.4.6 Sheath Formation

A simple plasma-etch reactor is shown in Figure 2.4. It consists of a grounded electrode which is typically connected to the chamber walls, a second electrode to which power is applied, and a partially evacuated chamber which contains a low pressure of a suitable mixture. Most systems use rf rather than dc power to avoid charge accumulation on insulator surfaces. The rf amplitude is in the range of 700-1000 V, and its frequency is typically 13.56 MHz. At such a frequency, most electrons oscillate between the electrodes, increasing the average electron energy and probability of electron-gas collisions. The rf power source is separated from the second electrode by a coupling capacitor to block dc current components. While the plasma chamber as a whole is neutral, recombination of charges at boundary surfaces surrounding the plasma causes charge depletion near these boundaries and the formation of a boundary layer called the sheath. The resulting gradient in charges gives rise to a net diffusion of carriers to the boundaries. Since electrons diffuse faster than ions, more electrons leave the plasma initially. Consequently, an excess of

positive ions is left in the plasma which now assumes a potential V_p with respect to the grounded walls.

The potential V_p gives rise to a drift current component which enhances the motion of ions and retards the motion of electrons to the grounded walls. When steady-state is reached, the electron and ion fluxes are balanced and the sheath is almost depleted of electrons. As a consequence of the reduced electron concentration, the sheath conductivity decreases considerably below that of the plasma region, and the probability for electron-gas collisions is reduced creating a "dark space" region.

The large difference between electron and ion mobilities also creates a sheath near the powered electrode. Since the coupling capacitor suppresses dc current components, electrons can accumulate at the electrode surface which assumes a negative dc voltage superimposed on the time-average AC potential. The powered electrode reaches a "selfbias" negative voltage, V_{DC} , with respect to ground (Coburn, 1982). Similarly, when an electrically isolated surface (such as an insulating substrate isolated from ground by an insulating film) is in contact with the plasma, it must receive equal electron and ion fluxes at steady state.

Following the same reasoning as above, the isolated surface must acquire a negative potential with respect to the plasma to retard the motion of electrons and enhance the motion of ions to equalize the fluxes of both carrier types. The potential of the isolated surface with respect to ground is referred to as its floating potential, V_F . As in the case of the grounded walls and the powered electrode, the isolated surface is surrounded by a sheath of reduced electron concentration. The sheaths are typically a few millimeters thick.

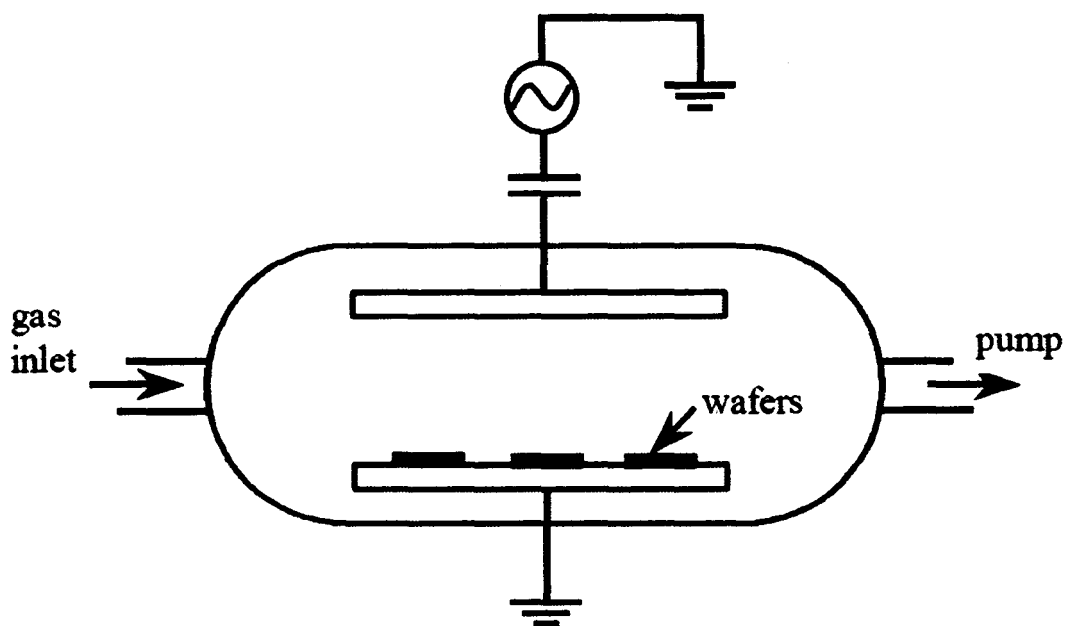


Fig. 2.4 Schematic of simplified plasma etch reactor.

2.4.6 Potential Distribution

The potential distribution in a plasma chamber is shown in Figure 2.5 for a two electrode parallel plate reactor, with rf power applied to one of the electrodes. The second electrode, which also includes the chamber walls, is at ground potential. The three time average potentials of importance are the plasma voltage (V_p), the “self-bias” voltage of the powered electrode (V_{DC}), and the floating voltage (V_F). They determine the energies of ions incident on floating surfaces in the plasma and their effect on etching (Coburn, 1982). For example, the difference between the plasma and floating potential determines the maximum energy with which ions bombard an electrically floating surface. The plasma, because of its degree of ionization and high conductivity, for practical purposes can be regarded as an equipotential volume. It assumes the highest potential of the system, V_p . Most of the voltage drops across the sheath because of its high resistance. The sheaths can be